

First principles study of structure, electronic and optical properties of $Y_3Fe_5O_{12}$ in cubic and trigonal phases

SHEN TAO^{1,2*}, HU CHAO², DAI HAILONG², YANG WENLONG², LIU HONGCHEN³, WEI XINLAO¹

¹Key Laboratory of Engineering Dielectrics and Its Application, Ministry of Education, Harbin University of Science and Technology, Harbin 150080, China

²College of Applied Sciences, Harbin University of Science and Technology, Harbin 150080, China

³School of Electrical Engineering and Automation, Harbin Institute of Technology, Harbin 150001, China

First principles calculations have been performed to investigate the structure, electronic and optical properties of $Y_3Fe_5O_{12}$. Both the cubic and trigonal phases have been considered in our calculation. The calculated structural parameters are slightly larger than the experimental values. The band structures show that $Y_3Fe_5O_{12}$ in cubic and trigonal phases have direct band gaps of 0.65 and 0.17 eV. The calculations of dielectric function, absorption, extinction coefficient, refractive index, energy loss function and reflectivity are presented.

Keywords: $Y_3Fe_5O_{12}$; first principles; electronic structure; optical properties

© Wrocław University of Technology.

1. Introduction

In recent years, an increasing attention has been given towards the study of perovskite oxides with the formula $A_3B_5X_{12}$ because of their application in magneto-optical devices [1], lasers [2], and solid electrolytes [3]. Yttrium iron garnet ($Y_3Fe_5O_{12}$), or YIG, belongs to the class of garnet-type $A_3B_5O_{12}$. The crystal of YIG is described in the trigonal phase (space group R-3) [4] and cubic phase (space group Ia-3d) [5]. Recently, several works on improving the magnetic and electrical properties of YIG have been reported in the open literature [6–14]. K. Bouziane et al. [6] prepared $Y_3Fe_{5-2x}Al_xCr_xO_{12}$ samples by ceramic technique and found that the Fe^{3+} at 16a positions (octahedral sites) was substituted by Cr^{3+} , while the Fe^{3+} at 24d positions (tetrahedral sites) was replaced by Al^{3+} . W. Zhong et al. [7] reported a novel cathode material, $Y_{2.5}Ca_{0.5}Fe_5O_{12}$, which was used for intermediate temperature solid oxide fuel cells. K. T. Jacob et al. [8] investigated the thermodynamic, nonstoichiometry and defects of

$YFeO_3$, YFe_2O_4 and $Y_3Fe_5O_{12}$. They found that the predominant defects in $Y_3Fe_5O_{12-\sigma}$ are cation interstitials. B. Raneesh et al. [9] synthesized Yttrium iron garnet nanoparticles by sol-gel technique and investigated the nonlinear optical properties of YIG. H. Aono et al. [10] prepared the nano-sized magnetic YIG powder by bead milling and found that crystallite diameter influenced the heat generation ability. K. Praveena et al. [11] prepared Gd-doped $Y_3Fe_5O_{12}$ nanopowders by modified sol-gel route and found that the Gd dopant was effective in enhancing the microwave absorption properties. Majid Niaz Akhtar et al. [12] gave a comprehensive study on influences of synthesis methods on the properties of the $Y_3Fe_5O_{12}$. B. Raneesh et al. [13] synthesized the composites $(1-x)ErMnO_{3-x}Y_3Fe_5O_{12}$ by sol-gel technique and found that an increase in YIG concentration enhanced the magnetization of the composite. It was reported that Bi dopant decreased the saturation magnetization of $Y_3Fe_5O_{12}$ nanoparticles [14]. Additionally, considerable research studies, focused on the magnetic thin films, have been reported [15–17]. H. L. Wang et al. [15] investigated the strain-tunable magnetocrystalline anisotropy in YIG thin

*E-mail: taoshenchina@163.com

films. S. M. Hamidi *et al.* [16] reported an experimental study on magneto-optical Faraday rotation of Ce-doped YIG thin film incorporating gold nanoparticles. A. Sposito *et al.* [17] prepared a micrometer-thick $\text{Y}_3\text{Fe}_5\text{O}_{12}$ films on $\text{Y}_3\text{Al}_5\text{O}_{12}$ substrates by pulsed laser deposition (PLD) and found that YIG films deposited on YAG substrates had a narrower ferromagnetic resonance (FMR) linewidth when compared with the YIG/GGG samples.

A theoretical investigation of the electronic, structural and optical properties is an important step towards the potential applications. It is, therefore, surprising that the calculations of the physical properties of YIG are scarce. To our best of knowledge, first-principles based on density functional theory (DFT) offers an effective tool to conduct a theoretical investigation on the physical properties of the compounds. What's more, the cubic phase of YIG is the most frequently investigated by researchers, while the research on trigonal phase is rare. In the present work, we have performed a first-principles calculation of electronic, structural and optical properties of YIG. The cubic and trigonal phases of YIG have both been considered in our calculation.

2. Computational method and results

2.1. Computational method and model

First principles calculations of YIG were performed using density functional theory (DFT) within the generalized gradient approximation (GGA) with the correction of Perdrew-Burke-Ernzerhof for the exchange-correction potential employed in the Cambridge Sequential Total Energy Package (CASTEP) code [18, 19]. We used the Materials Visualizer to build the YIG model. The model of YIG is shown in Fig. 1. The $\text{Fe-}3d^64s^2$, $\text{Y-}4s^24p^64d^15s^2$, and $\text{O-}2s^22p^4$ were treated as the valence states. Ultrasoft pseudopotentials (USP) were introduced by Vanderbilt [20] in order to ensure the convergence with the lowest possible cutoff energy for the plane-wave basis set. Integration over the Brillouin zone was

performed via discrete summation over the special set of k-points using the Monkhorst-Pack method [22]. To ensure the convergence of the computed structures and energies, the Kohn-Sham orbitals were expanded into plane waves with a kinetic energy cut-off of 380 eV, and the Brillouin zone k point integration was performed with a $4 \times 3 \times 5$ grid size.

During the optimization, a total energy convergence of 0.5×10^{-6} eV/atom, Hellmann-Feynman ionic force of 0.01 eV/Å, maximum stress of 0.02 Pa, and maximum displacement of 0.5×10^{-3} Å were used.

We used the material studio visualizer to build the YIG model. The models of YIG in cubic and trigonal phases are shown in Fig. 1a and 1b, respectively. The electronic configuration of Fe atom in $\text{Y}_3\text{Fe}_5\text{O}_{12}$ is $3d^64s^2$. According to the Hund's rules, atoms at ground states tend to have as many unpaired electrons as possible and all of the electrons in singly occupied orbitals try to maximize the total spin by holding the same spin directions. Thus, the Fe^{3+} ion, which possesses five unpaired electrons in 3d state, belongs to the high spin state.

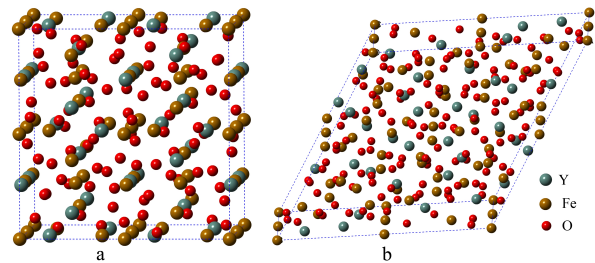


Fig. 1. The Ia-3d (a) and R-3 structure (b) of YIG.

2.2. Structural properties

The calculated lattice parameters of YIG in a cubic and trigonal phase are listed in Table 1. As shown in Table 1, the computed lattice parameter of cubic $\text{Y}_3\text{Fe}_5\text{O}_{12}$ (a) is 12.65 Å, which is 2.5 % larger than the experimental value. The lattice parameters acquired from the calculation of trigonal $\text{Y}_3\text{Fe}_5\text{O}_{12}$ ($a = 17.87$ Å and $c = 10.97$ Å) are 2.3 % larger than experimental values ($a = 17.48$ Å

and $c = 10.69 \text{ \AA}$). These results acquired from full structural relaxation of YIG are a bit larger when compared with the experimental values. The slight overestimation of the cell volume and lattice parameters is a typical feature of the GGA functional.

Table 1. Calculated and experimental lattice constants (\AA), in Ia-3d and R-3 structures.

| Space group | Present work | Experiment [4] |
|-------------|--------------|----------------|
| Ia-3d | | |
| a | 12.65 | 12.36 |
| R-3 | | |
| a | 17.87 | 17.48 |
| c | 10.97 | 10.69 |

2.3. Electronic properties

The GGA band structure, total (TDOS) and partial (PDOS) densities of states, which have been analyzed for both phases, are displayed in Fig. 2 and 3, respectively.

The calculated energy band structures of YIG in cubic and trigonal phases along the high symmetry directions in the Brillouin zone are shown in Fig. 2. Fermi levels are set as zero energy level for YIG. As shown in Fig. 2, the calculated band gaps for YIG in cubic and trigonal phases are 0.652 and 0.172 eV, respectively. The bottom of the conduction bands (CB) and the top of the valence bands (VB) are found to be 0 eV at G point and 0.65 and 0.17 eV at G points for cubic and trigonal phases, respectively, making both phases to be a direct band gap materials (G-G). It is well known that standard DFT calculation with current functionals have limited accuracy for band gaps, with underestimations larger than 1 eV being common when compared with the experimental data. Even the formally exact Kohn-Sham exchange-correlation function suffers from similar problems. It must be mentioned that the normal DFT calculation does not consider the electron correlation effect for transition metal 3d electrons, which results in an underestimated band gap. In transition metal systems, strong Coulomb repulsion

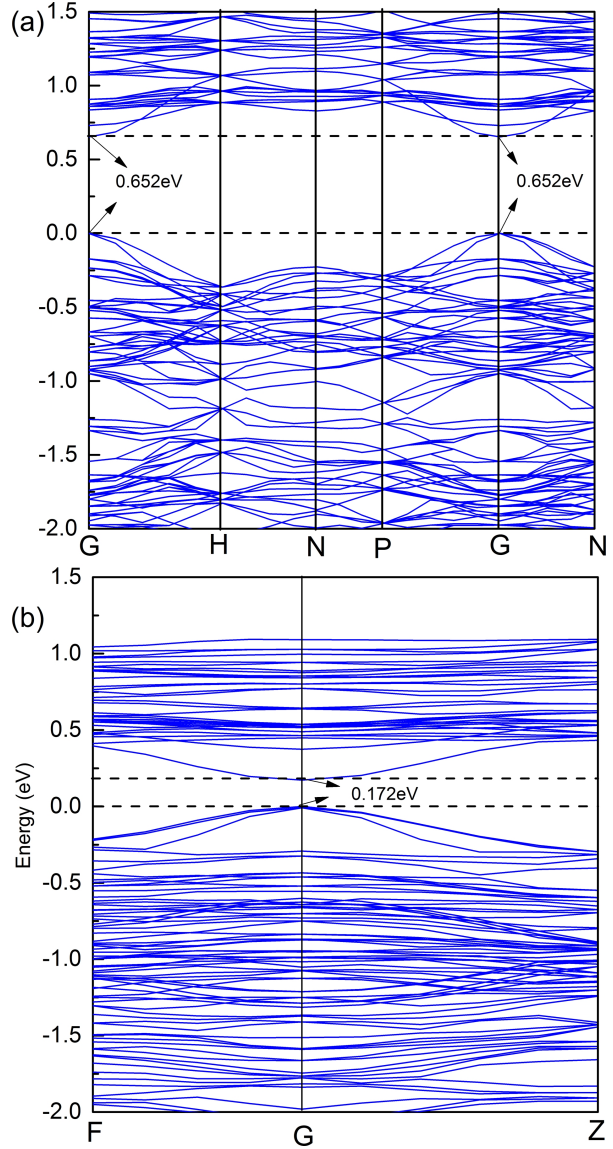


Fig. 2. Calculated band structures of YIG in Ia-3d (a) and R-3 structure (b).

between localized d orbitals is treated by introducing a Hubbard-like term to the effective potential, leading to a modified description of correlation effects (so called +U). However, the +U operation is dependent on the hardware requirement, and in comparison to the standard GGA (without +U), it is more time-consuming. X. T. Jia et al. [23] obtained the band structures of YIG in a cubic phase using GGA and GGA+U method with the band gap of 0.33 and 1.25 eV, respectively. It is sure that GGA (without +U) is sufficient to describe the

structural properties of YIG. Furthermore, the feature of optical spectrum was well described in the Kohn-Sham model by Jones despite the underestimated band gap [24]. An efficient way of dealing with the underestimated band gap is to make a rigid energy shift of conductive band to represent the experimental data (so called scissors operation).

Fig. 3 shows the calculated total and partial DOS of YIG in both phases. Since the features of PDOS of Ia-3d and R-3 phases are almost similar, for the sake of simplicity, we only discuss the PDOS of Ia-3d structure. From Fig. 3, the low valence bands in the range of -20 to -15 eV are contributed by O-s states and minor contribution of Y-d and Fe-d states. The upper valence bands in the range of -7 to 0 eV are mainly composed of O-p states hybridized with some Fe-3d and Y-3d electrons. The conduction band is predominantly occupied by Y-3d, Fe-3d and O-2p electrons. From the PDOS in Fig. 3, the O-2p electrons show a hybridization character with Fe-3d and Y-3d electrons, which suggests covalent bonding contribution in YIG. It is interesting to mention that the top of the valence bands reflects the p electronic character, mostly due to the O–O interaction.

2.4. Optical properties

To the best of our knowledge, the dielectric function is predominantly associated with the electronic response. The imaginary part $\varepsilon_2(\omega)$ of dielectric constant is derived from the real transition between the unoccupied electronic states and is given by [25]:

$$\varepsilon_2(\omega) = \frac{Ve^2}{2\hbar m^2 \omega^2} \int d^3k \sum_{ij} \langle ki | \vec{p} | kj \rangle^2 \cdot f(ki)(1 - f(kj)) \cdot \delta(E_{ki} - E_{kj} - \hbar\omega) \quad (1)$$

where e is the electric charge, \vec{p} is the dipole matrix and $ki(j)$ is the conduction (valence) band wave function corresponding to the i_{th} (j_{th}) eigenvalue with crystal momentum k . E_{ki} and $f(ki)$ are the energy of electron for the i_{th} state and the Fermi distribution function.

For the calculation of optical properties, a scissor operator should be used to fix the

underestimated band gap. Fig. 4 shows the dielectric function of YIG in cubic and trigonal phases. The imaginary or the absorptive part of the dielectric function $\varepsilon_2(\omega)$ is directly associated with the energy band structure. It is seen that the spectrum of $\varepsilon_2(\omega)$ for YIG phases shows two peaks. The major peak is located at around 3.8 eV/3.4 eV for cubic/trigonal phase corresponding to the transition from O-p electrons to Fe-3d and Y-3d states. The imaginary parts of the dielectric function for YIG cubic phase increase rapidly from 2.9 eV, forming the first peak, and the magnitude is much higher when compared with YIG trigonal phase. It indicates that YIG cubic phase shows a relatively high absorption.

The calculated absorption coefficient, extinction coefficient, refractive index, reflectivity and energy loss function are shown in Fig. 5. Gaussian smearing of 0.2 eV has been used in our calculation. The absorption edge starts from about 2.9 and 2.4 eV, corresponding to the fundamental energy gaps for YIG Ia-3d and R-3 phases, respectively. The absorption of YIG is very large (10^6 cm^{-1}) in the visible light region. As shown in Fig. 5a, the YIG Ia-3d phase has a higher absorption than the R-3 phase, which can also be reflected in the spectrum of $\varepsilon_2(\omega)$. The refractive index and extinction coefficient are shown in Fig. 5b and 5c. The static refractive indexes $n(0)$ of cubic and trigonal phases are 1.6 and 1.8, respectively. The $n(\omega)$ of trigonal phase increases in the infrared region forming a peak in the visible light area at about 2.8 eV, while the peak of $n(\omega)$ in the cubic structure is located at around 3.3 eV.

The reflectivity and energy loss function of fast electrons traversing our crystal correspond to each other, for instance, the major peak of the loss function corresponds to the trailing edge in the reflectivity spectrum. In cubic phase, the predominant peak of loss function is located at about 10.2 eV corresponding to the drastic reduction of the reflectivity. In trigonal phase, the sharp peak is situated at about 4.33 eV. Fig. 5e displays the reflectivity in both phases. As shown in Fig. 5e, in the range of 0 to 2.9 eV, the reflectivity is lower than 20 %, which indicates that YIG is a transparent material in the infrared.

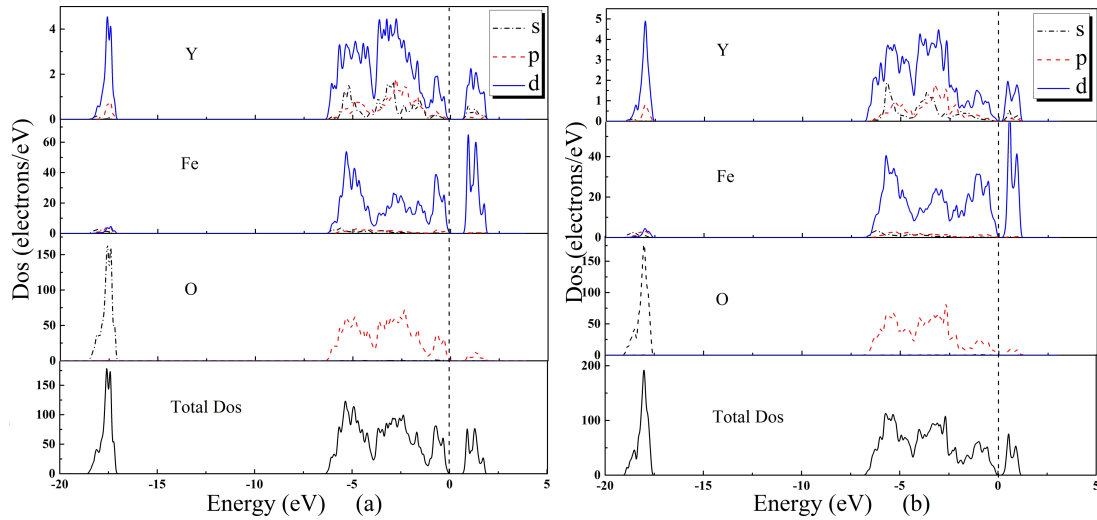


Fig. 3. Calculated density of states for YIG Ia-3d phase (a) and R-3 phase (b).

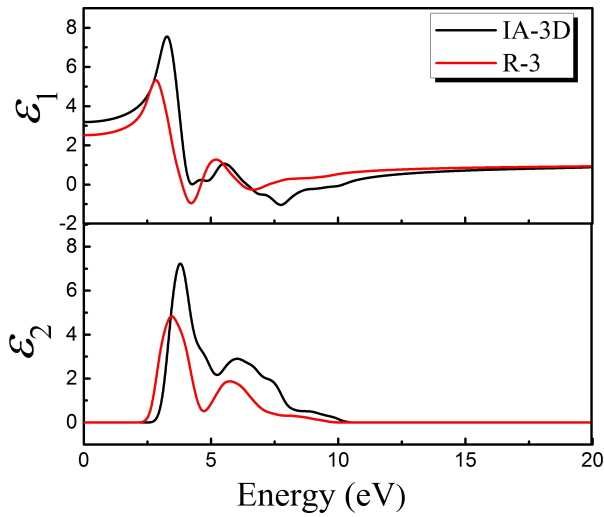


Fig. 4. The real part $\epsilon_1(\omega)$ (upper panel) and imaginary part $\epsilon_2(\omega)$ (lower panel) of the dielectric function of YIG phases.

3. Conclusions

In conclusion, the structural parameters, electronic structure and optical properties of YIG were investigated by using the first principles within the GGA. Our structural parameters were slightly larger than the experimental values. The calculated band structure showed that both phases of $Y_3Fe_5O_{12}$ had direct band gap (G-G). According to the analysis of density of states, the O-2p electrons show a hybridization character with Fe-3d and

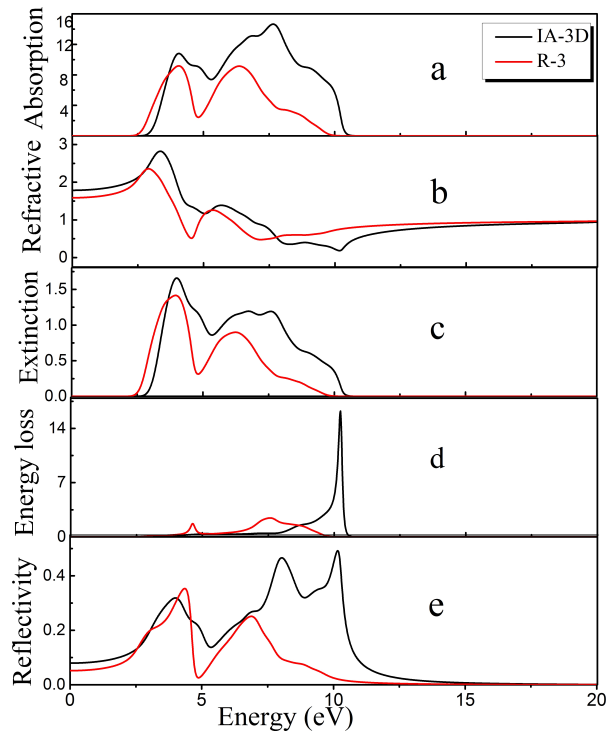


Fig. 5. Calculated absorption spectrum (a) ($\times 10^4/\text{cm}$), refractive index (b), extinction coefficient (c), energy loss function (d) and reflectivity (e) of YIG phases.

Y-3d electrons. To discuss the optical properties the dielectric function, absorption, refractive index, energy loss function and reflectivity have been calculated. The characteristics of optical spectrum of

YIG are influenced by the transition from the O-2p states (in the VB) to the Fe-3d and Y-3d states (in the CB). In the infrared, the low absorption and reflectivity indicate that YIG is almost transparent in this region.

Acknowledgements

The authors acknowledge financial support from National Natural Science Foundation of China (grant no. 51307036), Natural Science Foundation of Heilongjiang (grant no. E201303) and the Education Department of Heilongjiang (12531134)

References

- [1] VAQUEIRO P., LÓPEZ-QUINTELAA M.A., RIVASA J., GRENECHEB J.M., *J. Magn. Magn. Mater.*, 169 (1997), 56.
- [2] KIRANMALA L., REKHA M., NEELAM M., *Mater. Sci.-Poland*, 29 (2011), 184.
- [3] IMAGAWA H., OHTA S., KIHIRA Y., ASAOKA T., *Solid State Ionics*, 262 (2014), 609.
- [4] RODIC D., MITRIC M., TELLGREN R., RUNDLOF H., KREMENOVIC A., *J. Magn. Magn. Mater.*, 191 (1999), 137.
- [5] BONNET M., DELAPALME A., FUESS H., THOMAS M., *Acta Crystallogr. B*, 31 (1975), 2233.
- [6] BOUZIANE K., YOUSIF A., WIDATALLAH M.H., AMIGHIAN J., *J. Magn. Magn. Mater.*, 320 (2008), 2330.
- [7] ZHONG W., LING Y., RAO Y.Y., PENG R., LU Y.L., *Solid State Ionics*, 213 (2012), 140.
- [8] JACOB K.T., RAJITHA G., *Solid State Ionics*, 224 (2012), 32.
- [9] RANEESH B., REJEENA I., REHANA P.U., RADHAKRISHNAN P., SAHA A., KALARIKKAL N., *Ceram. Int.*, 38 (2012), 1823.
- [10] AONO H., EBARA H., SENBA R., NAOHARA T., MAEHARA T., HIRAZAWA H., WATANABE Y., *J. Magn. Magn. Mater.*, 324 (2012), 1985.
- [11] PRAVEENA K., SRINATH S., *J. Magn. Magn. Mater.*, 349 (2014), 45.
- [12] AKHTARA M.N., KHAN M.A., AHMAD M., MURTAZA G., RAZA R., SHAUKAT S.F., ASIF M.H., NASIR N., ABBAS G., NAZIR M.S., RAZAG M.R., *J. Magn. Magn. Mater.*, 324 (2012), 1985.
- [13] RANEESH B., SOUMYA H., PHILIP J., THOMAS S., NANDAKUMAR K., *J. Alloy. Compd.*, 611 (2014), 381.
- [14] YANG H.T., XU W., YU L.X., *Curr. Appl. Phys.*, 8 (2008), 1.
- [15] WANG H.L., DU C.H., HAMMEL P.C., YANG F.Y., *Phys. Rev. B*, 89 (2014), 134404.
- [16] HAMIDI S.M., TEHRANCH M.M., *J. Supercond. Nov. Magn.*, 25 (2012), 2713.
- [17] SPOSITO A., MAY-SMITH T.C., STENNING G.B.G., DE GROOT P.A.J., EASON R.W., *Opt. Mater. Express*, 3 (2013), 624.
- [18] PERDEW J.P., CHEVARY J.A., VOSKO S.H., JACKSON K.A., PEDERSON M.R., SINGH D.J., *Phys. Rev. B*, 46 (1992), 6671.
- [19] SEGALL M.D., LINDAN P.J.D., PROBERT M.J., PICKARD C.J., HASNIP P.J., CLARK S.J., PAYNE M.C., *J. Phys.-Condens. Mat.*, 14 (2002), 2717.
- [20] VANDERBILT D., *Physical Review B*, 41 (1990), 7892.
- [21] KRESSE G., HAFNER J., *J. Phys.-Condens. Mat.*, 6 (1994), 8245.
- [22] MONKHORST H.J., PACK J.D., *Phys. Rev. B*, 13 (1976), 5188.
- [23] JIA X.T., LIU K., XIA K., BAUER G.E.W., *EPL-Europhys. Lett.*, 96 (2011), 17005.
- [24] JONES R.O., GUNNARSSON O., *Rev. Mod. Phys.* 61 (1989), 689.
- [25] SAHA S., SINHA T.P., *Phys. Rev. B*, 62 (2000), 8828.

Received 2014-08-21
Accepted 2014-10-30